Synthesis and Characterization of GaN/quartz Nanostructure using Pulsed Laser Ablation in Liquid

Makram A Fakhri (mokaram_76@yahoo.com)
University of Technology-Iraq https://orcid.org/0000-0001-9010-6121
Husam Aldin A. Abdul Amir
Ali. A. Alwahib
Evan T. Salim
Forat H. Alsultany

Research Article

Keywords: Gallium nitride, Deposition by pulse laser ablation, X-Ray Diffraction (XRD), TEM, AFM, FESEM

Posted Date: February 25th, 2022

DOI: https://doi.org/10.21203/rs.3.rs-1370863/v1

Abstract

This study involves synthesizing gallium nitride (GaN) nanoparticles (NPs) under six different ablation energies using the pulsed laser ablation method. The nanoparticle was deposited using drop cast method on a quartz substrate. XRD pattern shows two peaks of h-GaN nanoparticles at 2θ = 34.64 and 37.98, reflected from (002) and (100) planes. The morphological properties indicate the hexagonal crystal nature of GaN that shows in the XRD pattern. Photoluminescence (PL) spectra show the highest laser power, 2000 mj has a minor emission peaked at 3.34 eV. The maximum emission peak 3.83 eV at 1400 mJ. The study depends on the pulsed laser to generate nanoparticles with different characteristics.

Introduction

Advanced electronic systems have been applied in optical devices depending on significant work that has been done for decades on large bandgap materials. These devices can typically be controlled at higher temperatures, higher voltages, and higher power densities, making them extremely interesting for future electronic systems [1, 2].

Due to its direct-wide band gap (3.4eV) and high thermal conductivity [3, 4], thermal stability, high melting point [5], high electron mobility [6], mechanical hardness, and high breakdown voltage [7], the material gallium nitride (GaN) has become more attractive in recent years. Due to these properties, thin film has become one of the essential materials of industrial devices.

Gallium nitride (GaN) high thermal conductivity material that makes it ideal for use in different sensors applications [8–10] solar cells [11, 12], light-emitting diode devices [13, 14], short wavelength optical devices [15, 16], high-power transistors [17, 18], and beta-voltaic devices [19].

Several studies have attempted to synthesize GaN nanostructures using various growth techniques, including metal-organic chemical vapor deposition[20], reactive molecular beam epitaxy [21], thermal ammonization [22, 23], physical vapor deposition [24, 25], chemical vapor deposition (CVD) [26], sol-gel chemistry [27], electrochemical deposition [28], thermal vapor deposition [29], and pulsed laser deposition (PLD) [30]. These methods have a common drawback in high temperatures and costly chemicals, leading to a relatively low production yield. Therefore, pulsed laser ablation in liquid (PLAL) [31] has recently improved the high quality of GaN films. This technique has been commonly used in the past to prepare thin films for high-quality multicomponent oxide ceramics. PLA is a perfect growth approach with many benefits over other methods, such as being very easy to operate, having no toxic or costly precursors, and thin film can be achieved at room temperatures [32, 33].

In this research involves synthesizing high-quality gallium nitride (GaN) nanoparticles (NPs) under six different ablation energies using the pulsed laser ablation method and deposited on the quartz substrates for fabricating high-quality optoelectronic devices and gas sensors.

Experimental Detail

In the experimental part, Fig. 1(a), shows a GaN target immersed in 5ml ethanol and shot with a Nd: YAG pulsed laser. The laser being used has a wavelength of 532 nm and a pulse repetition rate of 4 Hz. For each flowing energy one sample was prepared: 1000 mJ, 1200 mJ, 1400 mJ, 1600 mJ, 1800 mJ, and 2000 mJ. Each sample was irradiated with 500 pulses to saturate the nanomaterials liquid. The focal length varies after every 100 pulses to maintain the interaction between the laser energy and the GaN surface. The focal length at the start was 12 cm. Figure 1(b) depicts the liquid sample after laser ablation; the preparation conditions associated with this sedimentation process are listed in Table (1).

Table (1): PLA in liquids conditions.

Conditions	Values of PLAL
Laser wavelength	532nm
No. of pulses	500 shots
Pulse repetition rate	4 HZ
Energy	1000-2000 mJ
Distance between sample & target	12cm
Spot size	2mm
Pulse duration	10ns

As shown in Fig. 2, the GaN liquid samples were deposited onto the quartz substrate using a drop-casting process. A hotplate heated the quartz layer at a range of temperatures from (70^{o}C -90^{o}C). When the appropriate temperature was reached, nano-liquid was slowly dropped on the quartz substrate; each drop on the quartz substrate was left to dry and then followed by another drop (100 drops) to form the thin film GaN on the quartz substrate,the same process have been done for all the samples. The processes were performed in less than 12 hours to prevent oxidation during deposition. Before beginning the falling process with alcohol, the quartz substrate was thoroughly washed. Before each drop, the nano-liquid should be sufficiently shaken to preserve the GaN nanomaterials.

The quartz/nanoparticles (GaN) sample was tested in the XRD test, TEM, AFM, FESEM, PL. All results are analyzed in the next section of results and discussions.

Results And Discussions

3-1- Structural properties

Figure 3 presents the XRD GaN nanoparticles synthesized and drop-casted on quartz substrate at different ablation energies (1000, 1200, 1400, 1600, 1800, and 2000mj). The diffraction peaks in the XRD pattern are matched with standard cubic and wurtzite hexagonal structures of the GaN crystal. The nanoparticles prepared for 1000mj exhibit h-GaN rise at 2θ = 34.64 reflected from (002) plane and c-GaN

peak at 2θ = 40.22 reflected from (111) plane cubic phase has affected the peak intensity and the sharpness of the hexagonal phase. The sample of 1200mj displays h-GaN nanoparticles at 2θ = 34.64 and 37.98, which are reflected from (002) and (100) planes. The intensity and the sharpness of the peak begin to increase with increasing the ablation energy. The third sample of 1400mj shows two peaks of h-GaN nanoparticles at 2θ = 34.64, and 37.98 reflected from (002) and (100) planes, the intensity of the peak increased due to increase the structure crystallization. The fourth sample of 1600mj displays h-GaN nanoparticles at 2θ = 34.64 and 37.98, which is reflected from (002) and (100) planes; this sample has the highest peak due to the excellent quality of h-GaN nanoparticles. The fifth sample of 1800mj shows two peaks of h-GaN nanoparticles at 2θ = 34.64 and 37.98, which reflected from (002) and (100) planes, the peak intensity begins to decrease due to decreasing the structure crystallization, and the sixth sample of 2000 mJ shows two peaks of h-GaN nanoparticles at 2θ = 34.64 and 37.98 which reflected from (002) and (100) planes, the intensity of the peak is less than the fifth sample. This indicates high intensity in response to the excellent quality of h-GaN nanoparticles synthesized in the fourth sample at low temperature.

Furthermore, it is shown that the intensity of the peaks for the XRD pattern increased with increasing laser ablation energy due to increasing of the grain size and concentration of ablated material and due to enhancement of crystal quality until (1600 mJ) that has the highest intensity peak then the intensity peak back to decrease as the laser ablation increase.

3-2- Morphological properties

3-2-1 AFM results

This section includes a profound discussion of the results. Figure 4 presents AFM images of the GaN nanophotonic; the change in the root mean square and roughness and grain size of the GaN nanophotonic, with the difference in the pulsed laser ablation energy are shown in Table 1. The GaN nanoparticles prepared for 1000mj exhibit high root mean square (23.40nm) and roughness (3.750nm). The sample of 1200 mJ displays root mean square (16.00nm) and roughness of (4.533nm). The sample of 1400mj and 1600mj shows the highest roughness. The smallest root mean square due to the excellent quality of the structure crystallization and high regular crystals distribution, the roughness back to decrease, and the root mean square increase cause the reduction in the structure crystallization and regular crystals distribution 1800 mJ and 2000mJ [5].

Table 1: AFM data of GaN/quartz nanostructures at different ablation energies.

Laser ablation energy (mj)	Roughness (nm)	Root-mean-square value (nm)	Grains (nm)
1000	3.750	23.40	27. 29 - 116.6
1200	4.533	16.00	12.57 - 103.7
1400	5.871	5.640	4.361 - 58.88
1600	4.984	11.40	9.183 - 69.44
1800	4.575	14.168	4.196 - 88.51
2000	3.260	19.88	10.07 - 158.7

Figure 5 represents the relation between the grains density and the grains size at different ablation energies. The GaN nanoparticles prepared for 1000mj exhibit a wide range of grain size (27. 29 nm – 116.6nm) with grains density (0.002). The sample 1200 mJ display a range of grain size (12.57 nm-103.7nm), the range of grain size decrease and the grains density increase. The samples of 1400 mJ and1600 mJ show the smallest range of grain size (4.361nm-58.88nm) and (9.183nm-69.44nm) and the highest grains density due to high regular crystals distribution, then the density of the grain back to decrease at 1800 mJ because of the decrease in the regularity of the distribution of the crystal and then back to increase at 2000 mJ due to regular crystals distribution [5].

3-2-2 FESEM results

Figure 6 presents the FESEM images and the EDX spectrum of GaN nanoparticles for the six samples synthesized under different ablation energies. These samples were built using a drop cast on the quartz substrate. The EDX spectra of GaN nanoparticles have both elements Ga, and N. The [Ga]/N ratio depends on laser ablation energy. At 1000 mJ, FESEM image shows the beginning of the crystallization process, and the ratio of [Ga] / [N] was 5. The second sample at 1200 mJ exhibits an increase in the structure crystallization. The ratio of [Ga] / [N] was 3.77. The third sample of 1400 mJ shows improves crystallization than the second sample; the ratio of [Ga] / [N] was 3.633. The fourth sample at 1600 mJ shows a good crystallization quality, the ratio of [Ga] / [N] was 4.19. The fifth sample at 1800 mJ exhibits several particles to be agglomerated; the ratio of [Ga] / [N] was 3. The sixth sample at 2000 mJ shows an increase in the number of agglomerated particles with increasing the laser ablation energy, the ratio of [Ga] / [N] was 3.45.

Moreover, FESEM images showed that the crystallization of GaN nanoparticle increased with increasing laser ablation energy due to increased grain size, the concentration of ablated material becoming higher, and the enhancement of crystal quality until (1600 mJ), and this in good agreement with XRD result. Increasing the laser ablation energy above 1600 mJ will make the particles agglomerated, and the number of agglomerated particles will increase with increasing the laser ablation energy.

3-2-3 TEM results

TEM was performed to obtain a submicroscopic image of the nanoparticles of less than 100nm. Figure 7a shows the 1000 mJ indicates that the GaN nanoparticles have quasi-spherical particles with grain size varies from 27.29nm to116.6nm. Figure 7b at 1000 mJ, the sample exhibited a good crystallization quality with the lowest grain size ranging from 4.361nm to 58.88nm. Figure 7c prepared for 1800 mJ shows grain size varies from 4.196nm to 88.51nm; the particles began to agglomerate with increasing the laser ablation energy. The TEM images support the FESEM images of GaN. The FESEM with EDX and TEM also validated the GaN nanoparticles' chemical purity earlier shown with the XRD data. Therefore, it can be inferred that ablation energy is crucial in the synthesis GaN nanoparticles.

3-3- Optical properties

Figure 8 demonstrates the photoluminescence (PL) spectra of the prepared GaN under different laser ablation energies. The energy of the incident photon ($E = hv$) as a function of the wavelength (λ) was calculated using Eq. (1)

$$Eg = \frac{1240}{\lambda}$$

1

The first GaN nanoparticle prepared for 1000 mJ presents an energy gap of 3.38 eV at the wavelength 366nm. The second sample prepared for 1200mj exhibits an energy gap of 3.41 eV at the wavelength 363nm. The energy gap increases with increasing the ablation energy, and the wavelength will have a blue shift. The third sample prepared for 1400 mJ presents an energy gap of 3.83 eV at the wavelength 323 nm; this sample has the highest energy gap due to the small piratical size and the blue shift. The fourth sample prepared for 1600 mJ exhibits an energy gap of 3.71 eV at 334 nm. The energy gap began to decrease with increasing the ablation energy that will ablate large piratical size, and the wavelength will have redshift. The fifth sample prepared for 1800 mJ exhibit an energy gap of 3.54 eV at the wavelength 350 nm; the wavelength will have a redshift, and the energy gap decrease. The sixth sample prepared for 2000mj present the smallest energy gap of 3.34 eV at the wavelength 371nm; the wavelength will have redshift, the photoluminescence (PL) investigation proved the AFM result.

Furthermore, It can be seen that increasing the ablation energy will remove the larger particle size, and therefore, the wavelength will have a red shift, So decreasing the ablation energy will make a blue shift in the wavelength and increase the energy gap until 1400mj that has the highest peak of power then at 1200 and 1000 mJ the energy gap decrease and wavelength will have redshift due to the core-shell phenomenon.

Conclusion

This paper presents the synthesis of gallium nitride (GaN) nanoparticles (NPs) under six different ablation energies using pulsed laser ablation method. GaN deposited on the quartz substrate analyzed using XRD, AFM, FESEM, TEM, and PL tests. XRD test indicates high intensity in response to the excellent

quality of h-GaN nanoparticles synthesized in the fourth sample. The morphological properties (AFM, FESEM, and TEM) inferred that ablation energy is a critical factor in the synthesis GaN nanoparticles. Photoluminescence (PL) spectra proved that decreasing the ablation energy will make a blue shift in the wavelength and increase the energy gap until 1400 mJ, the highest peak of energy at 1400 mJ. The energy gap decrease and wavelength will have redshift due to the core-shell phenomenon.

Declarations

Ethics approval and consent to participate

(Not applicable)

Consent for publication

(Not applicable)

Availability of data and materials

(Not applicable)

Competing interests

The authors have declared that no competing interests exist

Funding

No fund has been received for this research study.

Authors' contributions

Makram and Evan conceived of the presented idea

Makram and Ali supervised the finding of this work

All authors discussed the results and contributed equally to the final manuscript.

Ali , Husam , Evan, and Forat conducted the experiments

All authors provided critical feedback and helped shape the research, analysis and manuscript.

Conflict of interest

The authors have declared no conflict of interest.

Acknowledgment

The authors would like to thank the department of laser engineering and electro- optic /university of Technology for the logistic support this work.

Corresponding author: Assoc. Prof. Dr. Makram A. Fakhri.

References

1. L. Sang, M. Liao, and M. Sumiya, “A comprehensive review of semiconductor ultraviolet photodetectors: from thin film to one-dimensional nanostructures,” *Sensors*, vol. 13, no. 8, pp. 10482–10518, 2013.
2. R. Velazquez, A. Aldalbahi, M. Rivera, and P. Feng, “Fabrications and application of single crystalline GaN for high-performance deep UV photodetectors,” *AIP Adv.*, vol. 6, no. 8, p. 85117, 2016.
3. S. Mani, N. Yadava, and R. K. Chauhan, “Performance Comparison of Different Buffer/Substrate Material Combination based Ultra Bright Blue LED,” in *2020 International Conference on Electrical and Electronics Engineering (ICE3)*, 2020, pp. 508–512.
4. N. K. R. Nallabala *et al.*, “Structural, optical and photoresponse characteristics of metal-insulator-semiconductor (MIS) type Au/Ni/CeO2/GaN Schottky barrier ultraviolet photodetector,” *Mater. Sci. Semicond. Process.*, vol. 117, p. 105190, 2020.
5. A. Mantarcı, “Structural, Morphological, and Optical Characterization of GaN/p-Si Thin Films for Various Argon Flow Rates,” *JOM*, vol. 72, no. 1, pp. 552–560, 2020.
6. X. G. He *et al.*, “GaN high electron mobility transistors with AlInN back barriers,” *J. Alloys Compd.*, vol. 662, pp. 16–19, 2016.
7. W. Saito, T. Suwa, T. Uchihara, T. Naka, and T. Kobayashi, “Breakdown behaviour of high-voltage GaN-HEMTs,” *Microelectron. Reliab.*, vol. 55, no. 9–10, pp. 1682–1686, 2015.
8. A. Acharyya, “Gallium Nitride-Based Solid-State Devices for Terahertz Applications,” *Adv. Mater. Futur. Terahertz Devices, Circuits Syst.*, vol. 727, p. 9, 2021.
9. Z. Zheng *et al.*, “Gallium nitride-based complementary logic integrated circuits,” *Nat. Electron.*, vol. 4, no. 8, pp. 595–603, 2021.
10. S. Sankaranarayanan, P. Kandasamy, R. Raju, S. Gengan, and B. Krishnan, “Controlled growth of gallium nitride nanowires on silicon and their utility in high performance Ultraviolet-A photodetectors,” *Sensors Actuators A Phys.*, vol. 332, p. 113189, 2021.
11. V. Chandra, A. D. D. Dwivedi, and N. Sinha, “TCAD based performance assessment of Indium Gallium Nitride based single junction solar cells for different mole fractions of Indium,” *Opt. Quantum Electron.*, vol. 53, no. 2, pp. 1–15, 2021.
12. N. K. R. Nallabala *et al.*, “High performance, self-powered and thermally stable 200–750 nm spectral responsive gallium nitride (GaN) based broadband photodetectors,” *Sol. Energy Mater. Sol. Cells*, vol. 225, p. 111033, 2021.

13. A. S. Hedzir, N. F. Hasbullah, and N. F. Hasbullah, “A review of high ideality factor in gallium nitride-based light-emitting diode,” *Semicond. Physics, Quantum Electron. Optoelectron.*, vol. 24, no. 1, pp. 83–89, 2021.
14. A. D. Griffiths, J. Herrnsdorf, J. J. D. McKendry, M. J. Strain, and M. D. Dawson, “Gallium nitride micro-light-emitting diode structured light sources for multi-modal optical wireless communications systems,” *Philos. Trans. R. Soc. A*, vol. 378, no. 2169, p. 20190185, 2020.
15. M.-H. Chen, W.-N. Chou, V.-C. Su, C.-H. Kuan, and H. Y. Lin, “High-performance gallium nitride dielectric metalenses for imaging in the visible,” *Sci. Rep.*, vol. 11, no. 1, pp. 1–8, 2021.
16. G. R. Goldberg *et al.*, “Gallium nitride light sources for optical coherence tomography,” in *Gallium Nitride Materials and Devices XII*, 2017, vol. 10104, p. 101041X.
17. Y. C. Lin *et al.*, “Gallium Nitride (GaN) High-Electron-Mobility Transistors with Thick Copper Metallization Featuring a Power Density of 8.2 W/mm for Ka-Band Applications,” *Micromachines*, vol. 11, no. 2, p. 222, 2020.
18. G. Meneghesso, M. Meneghini, and E. Zanoni, *Gallium nitride-enabled high frequency and high efficiency power conversion*. Springer, 2018.
19. M. R. Khan *et al.*, “Design and characterization of GaN pin diodes for betavoltaic devices,” *Solid. State. Electron.*, vol. 136, pp. 24–29, 2017.
20. Y. Zhang, Z. Chen, K. Zhang, Z. Feng, and H. Zhao, “Laser-Assisted Metal–Organic Chemical Vapor Deposition of Gallium Nitride,” *Phys. status solidi (RRL)–Rapid Res. Lett.*, vol. 15, no. 6, p. 2100202, 2021.
21. S. W. King, R. F. Davis, and R. J. Nemanich, “Gas source molecular beam epitaxy of scandium nitride on silicon carbide and gallium nitride surfaces,” *J. Vac. Sci. Technol. A Vacuum, Surfaces, Film.*, vol. 32, no. 6, p. 61504, 2014.
22. U. Rizal, B. S. Swain, and B. P. Swain, “The role of ammonization on chemical bonding and optical properties of nickel-catalyzed gallium nitride nanowire,” *Appl. Phys. A*, vol. 122, no. 4, p. 291, 2016.
23. M. Fathy, S. Gad, B. Anis, and A. E.-H. B. Kashyout, “Crystal Growth of Cubic and Hexagonal GaN Bulk Alloys and Their Thermal-Vacuum-Evaporated Nano-Thin Films,” *Micromachines*, vol. 12, no. 10, p. 1240, 2021.
24. K. M. A. Saron and M. R. Hashim, “Broad visible emission from GaN nanowires grown on n-Si (1 1 1) substrate by PVD for solar cell application,” *Superlattices Microstruct.*, vol. 56, pp. 55–63, 2013.
25. P. Rouf *et al.*, “Hexacoordinated Gallium (III) Triazenide Precursor for Epitaxial Gallium Nitride by Atomic Layer Deposition,” *Chem. Mater.*, vol. 33, no. 9, pp. 3266–3275, 2021.
26. V. Purushothaman and K. Jeganathan, “Structural evolution and growth mechanism of self-assembled wurtzite gallium nitride (GaN) nanostructures by chemical vapor deposition,” *J. Phys. Chem. C*, vol. 117, no. 14, pp. 7348–7357, 2013.
27. C. Y. Fong, S. S. Ng, F. K. Yam, H. A. Hassan, and Z. Hassan, “An investigation of sol–gel spin coating growth of wurtzite gan thin film on 6h–sic substrate,” *J. Cryst. Growth*, vol. 413, pp. 1–4, 2015.

28. A. I. A. Ali, H. T. Danga, J. M. Nel, and W. E. Meyer, “Deep-level transient spectroscopy of GaN grown by electrochemical deposition and irradiated with alpha particles,” *Mater. Sci. Semicond. Process.*, vol. 127, p. 105685, 2021.
29. J. Meng, S. Wong, and Y. Jaluria, “Fabrication of gallium nitride films in a chemical vapor deposition reactor,” *J. Therm. Sci. Eng. Appl.*, vol. 7, no. 2, p. 21003, 2015.
30. W.-K. Wang, S.-Y. Huang, M.-C. Jiang, and D.-S. Wuu, “Optoelectronic properties and structural characterization of GaN thick films on different substrates through pulsed laser deposition,” *Appl. Sci.*, vol. 7, no. 1, p. 87, 2017.
31. J. Hao, S. Xu, B. Gao, and L. Pan, “PL tunable GaN nanoparticles synthesis through femtosecond pulsed laser ablation in different environments,” *Nanomaterials*, vol. 10, no. 3, p. 439, 2020.
32. A. Demirel, T. Öztaş, C. Kurşungöz, İ. Yılmaz, and B. Ortaç, “Synthesis of blue-shifted luminescent colloidal GaN nanocrystals through femtosecond pulsed laser ablation in organic solution,” *J. Nanoparticle Res.*, vol. 18, no. 5, p. 128, 2016.
33. H. A. A. A. Amir, M. A. Fakhri, A. A. Alwahib, and E. T. Salim, “Synthesize of GaN/quartz Nanostructure Using Pulsed Laser Ablation in Liquid for Optoelectronic Devices,” 2021.

Figures

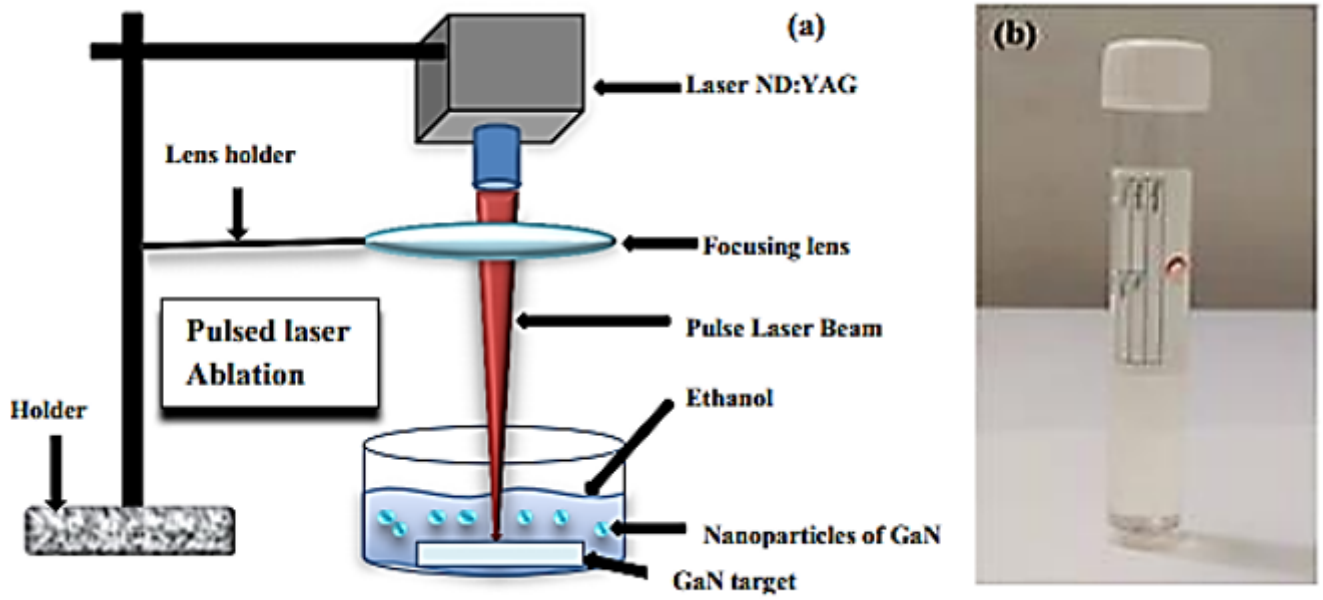

Figure 1

a) laser ablation method b) liquid sample generated from ablation method

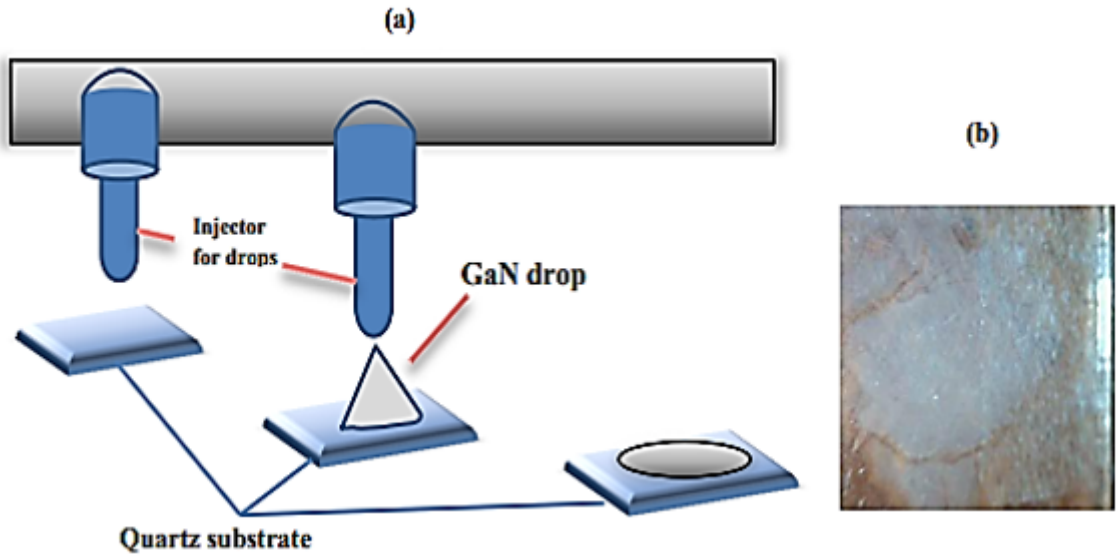

Figure 2

a) drop-casting method for GaN b) GaN/Quartz thin film

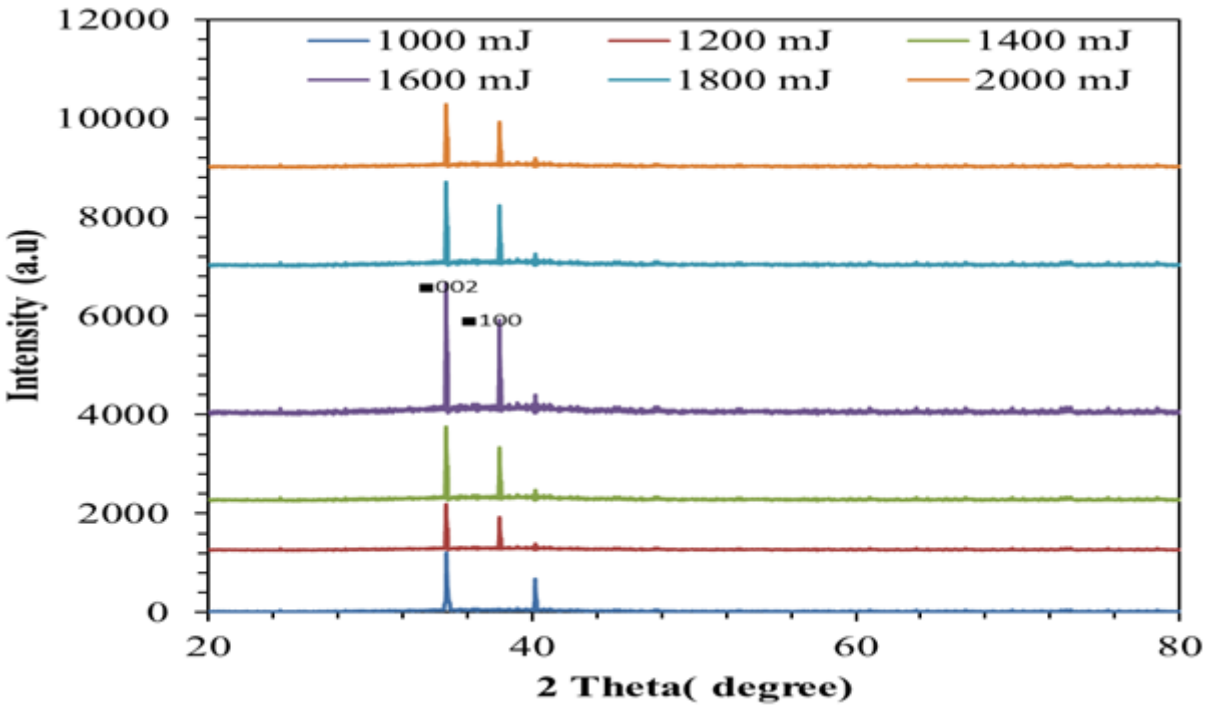

Figure 3

XRD patterns of GaN nanophotonic with different ablation energies

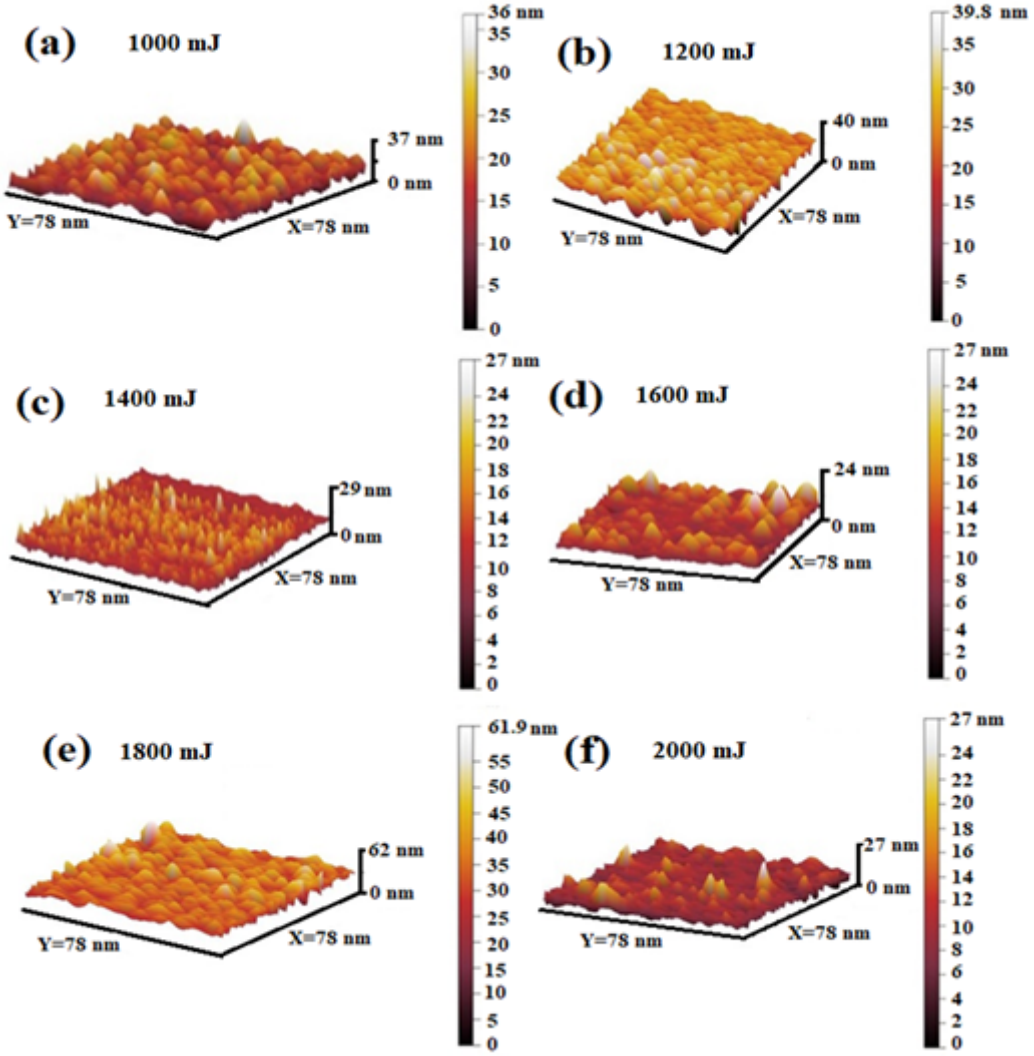

Figure 4

AFM images of GaN/quartz nanostructures at different ablation energies

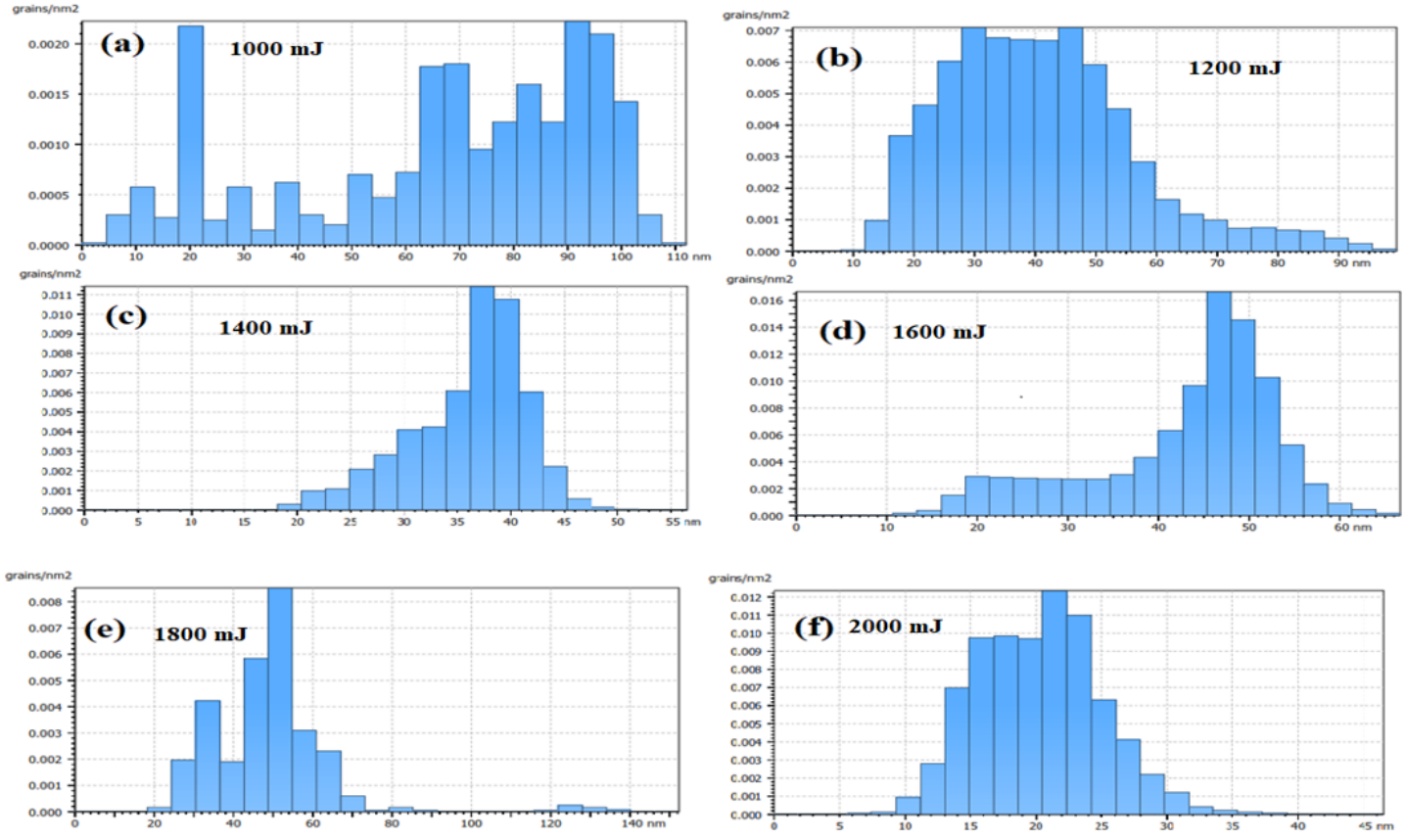

Figure 5

The average grain size curve of GaN/quartz nanostructures at different ablation energies

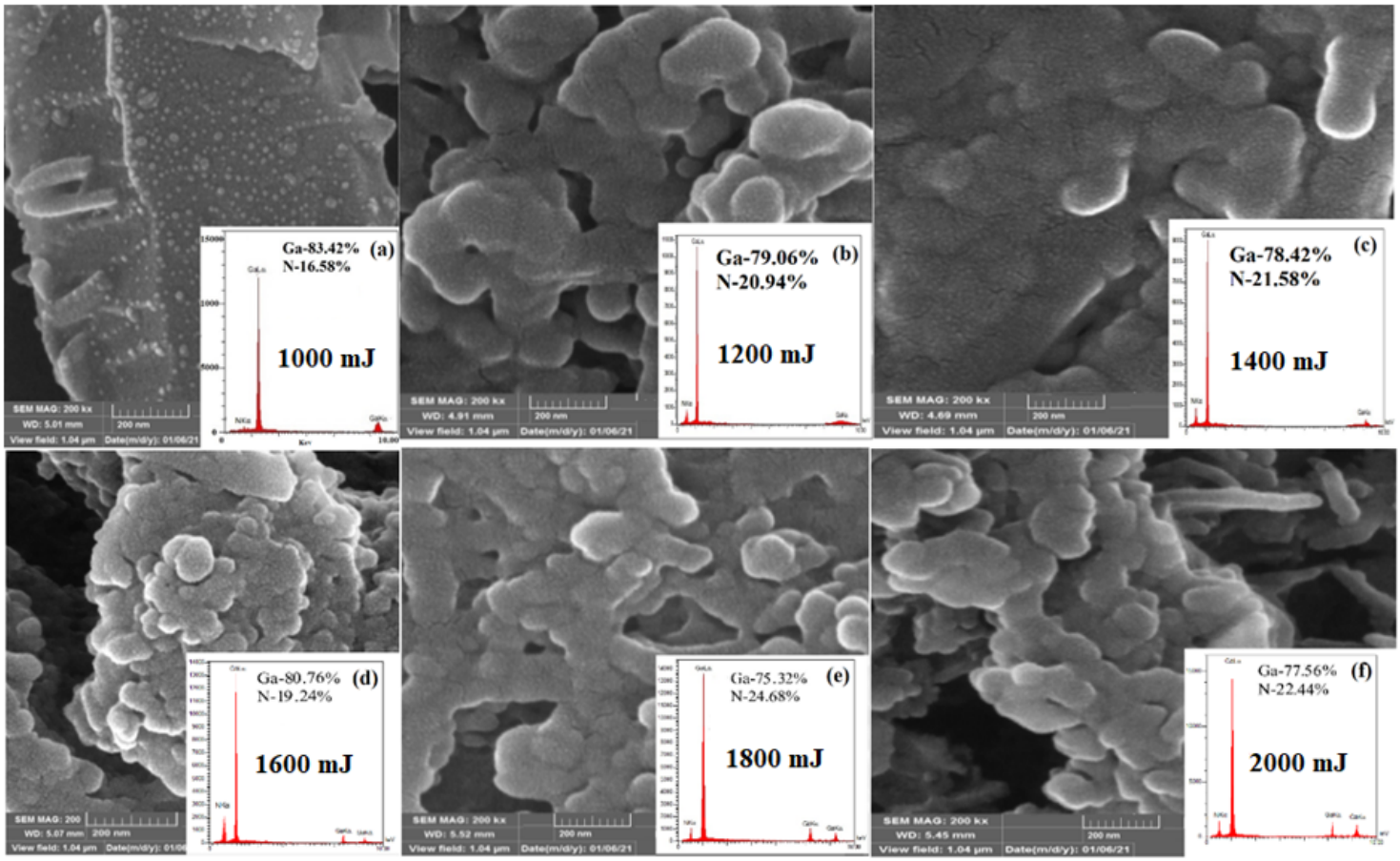

Figure 6

The FESEM images and EDX spectra of the GaN nanostructures grown on the quartz substrates at different ablation energies

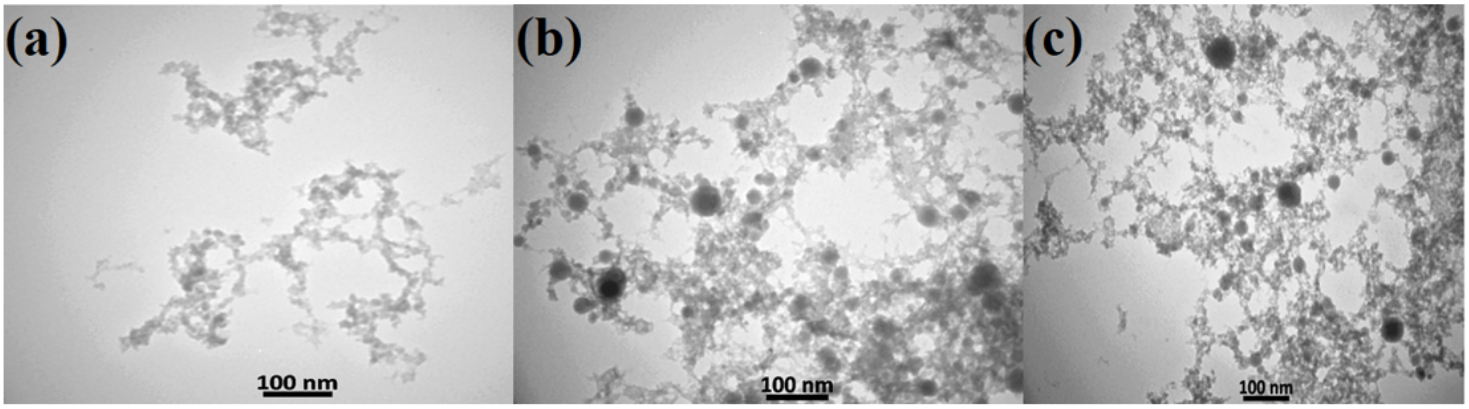

Figure 7

TEM images of the GaN nanostructures grown on the quartz substrates at different ablation energies (a) 1000 mJ, (b) 1400 mJ, and (c) 1800 mJ

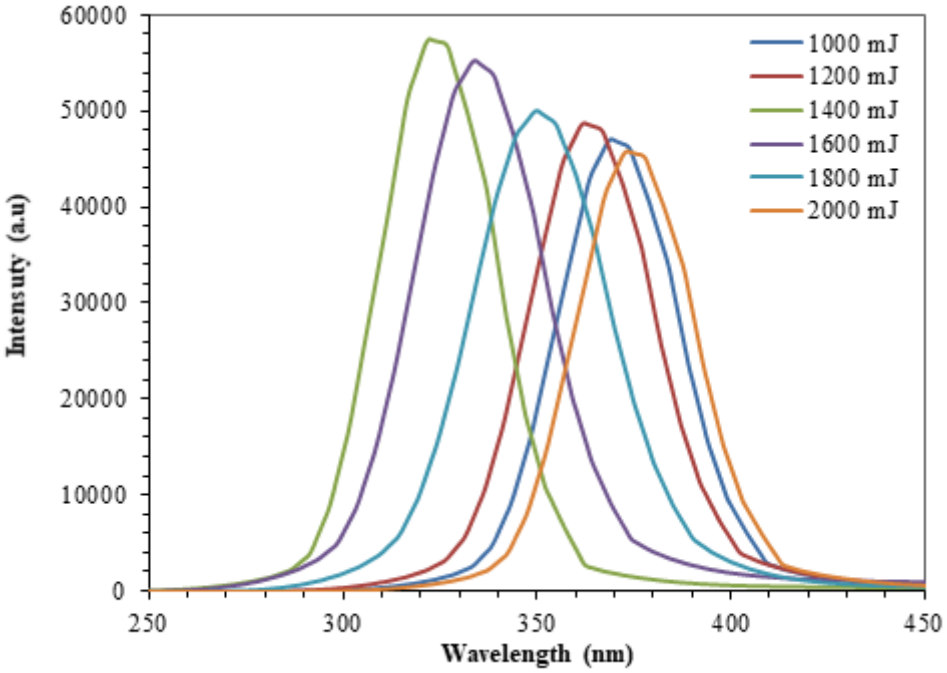

Figure 8

PL spectra of GaN at different ablation energies